Prospectivity Mapping for Turbidite-hosted Gold-Antimony (Au-Sb) Mineral Systems in Northeast Tasmania

Geological Survey Technical Report TR49

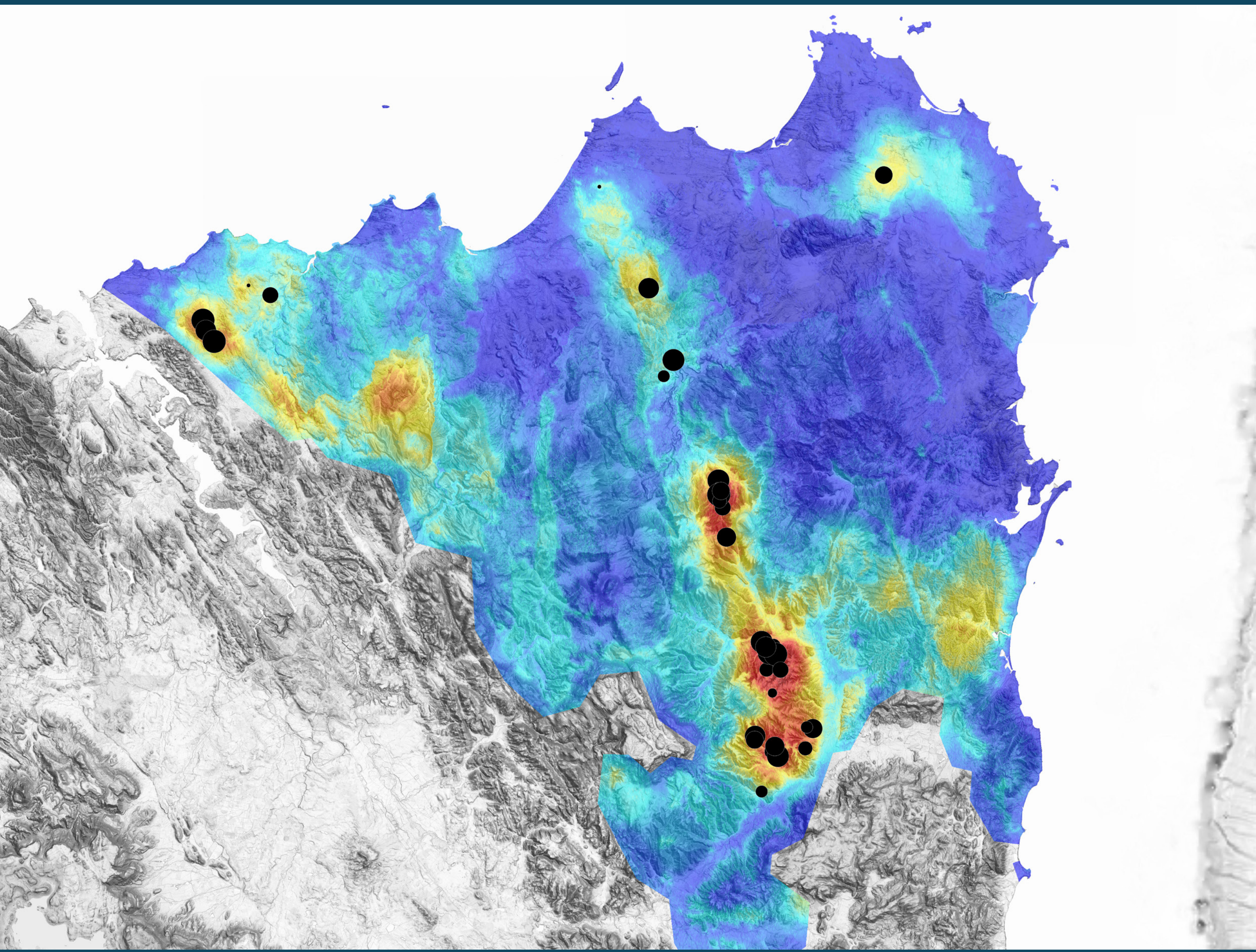

Mineral Resources Tasmania

Tasmanian Government

Geological Survey Technical Report 49:

Prospectivity Mapping for Turbidite-hosted Gold-Antimony (Au-Sb) Mineral Systems in Northeast Tasmania

by

T. Czertowicz

Cover: Gold-antimony prospectivity map and training points.

Executive Summary

This study presents machine learning-based prospectivity mapping for turbidite-hosted gold-antimony (Au-Sb) mineralisation across Tasmania, supporting the Tasmanian Government's Critical Minerals Strategy by identifying high-potential exploration targets for critical minerals essential for strategic developing technologies. Northeast Tasmania hosts several historic goldfields, including the Mathinna, Alberton, and Lefroy goldfields. Given the increasing strategic importance of antimony and the presence of analogous antimony-rich deposits in Victoria, reassessment of the region's prospectivity is warranted. This study represents the first application of machine learning to gold prospectivity mapping in northeast Tasmania, providing a new approach to assess the region's potential.

The prospectivity modelling used a mineral system approach that considers the large-scale geological processes responsible for mineral deposit formation. A total of 135 predictor maps were generated that represent source, transport, trap, and deposition processes. An ensemble random forest machine learning approach was used to integrate geological, geophysical, and geochemical datasets at 40 m resolution across northeast Tasmania. Two models were developed: (1) a geophysics-only model suitable for regional and greenfield targeting, and (2) a comprehensive model incorporating all available data for refined exploration targeting. Models were trained on 40 known deposits and validated using several independent techniques and expert geological feedback within Mineral Resources Tasmania.

Both models demonstrate strong predictive performance, with Model 2 capturing 95 % of known deposits within the top 12 % most prospective areas. Comparison with an independent set of gold deposits shows that the models can successfully predict mineralisation away from training data.

Predictor maps with the highest importance scores are consistent with the turbidite-hosted Au-Sb mineral system model, and include carbonaceous rocks, minor faults, Mathinna Supergroup host rocks, competency contrasts, and copper- and arsenic-rich stream catchments.

Both models highlight the Mangana-Mathinna-Alberton belt as the most prospective region, consistent with historical production and current exploration activity. Additional prospective areas include Lefroy, Forester, Lisle, Gladstone, and Upper Scamander. Some of these areas have received limited historical exploration and warrant further investigation.

These models reduce exploration search space by over 85 %, providing objective, data-driven evidence to improve exploration efficiency and inform land-use decisions. Results will guide resampling of legacy drill core to determine the critical mineral budgets of these systems. The methodology will be extended to other critical mineral-bearing systems across Tasmania with models updated as new data become available.

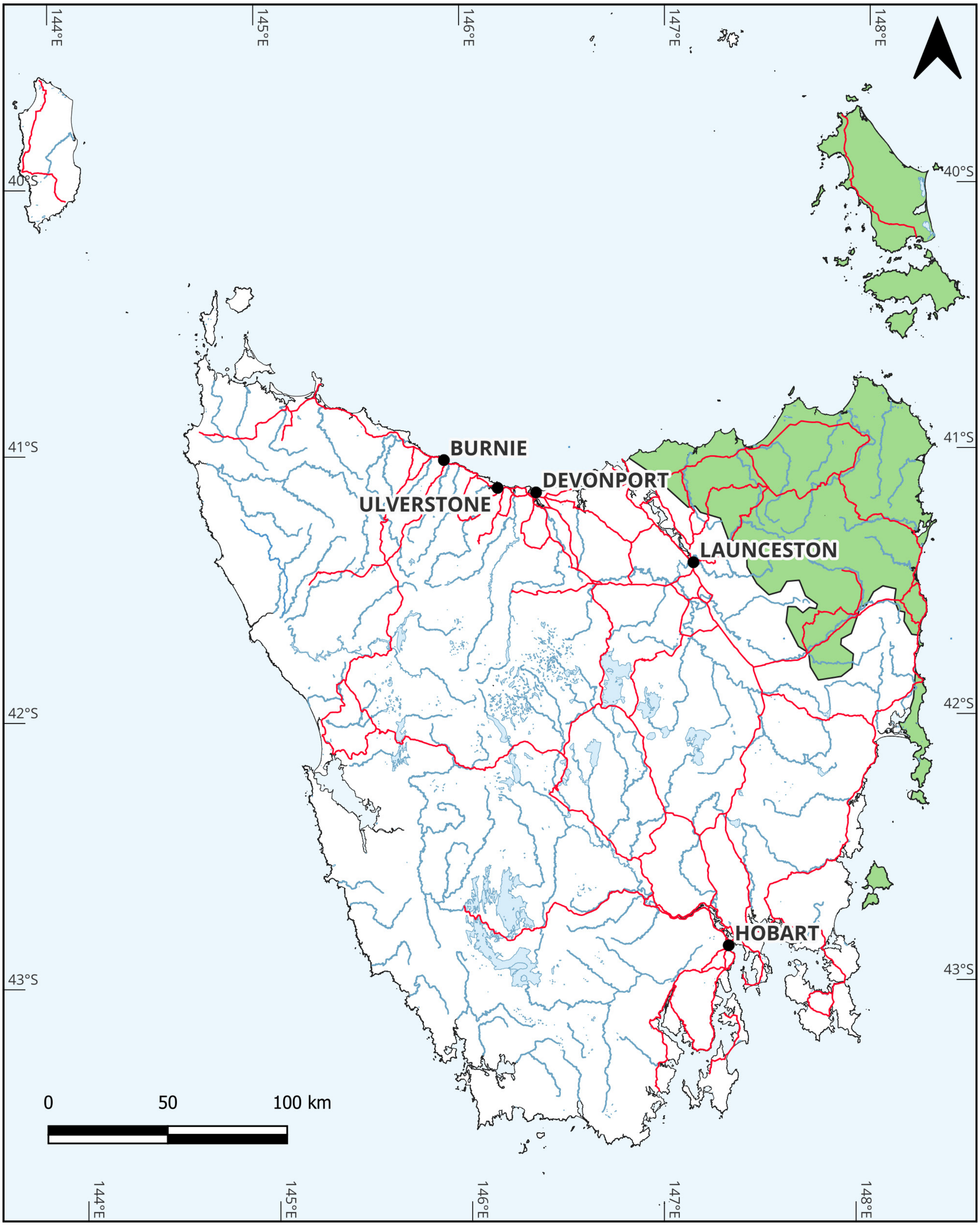

Project Location Map

Tasmanian Government

Mineral Resources Tasmania
www.mrt.tas.gov.au

Prospectivity Mapping for Turbidite-hosted Gold-Antimony (Au-Sb) Mineral Systems in Northeast Tasmania

by T. Czertowicz
Geological Survey Branch - Mineral Resources Tasmania

CONTENTS

FIGURES

TABLES

1.0 INTRODUCTION

This report presents prospectivity mapping for turbidite-hosted gold-antimony (herein Au-Sb) mineralisation in northeast Tasmania using machine learning, a mineral systems approach, and diverse geoscientific datasets to identify areas of high mineral potential.

This work supports global efforts to identify and develop critical mineral resources to support future technologies and the green energy transition. The Tasmanian Government's Critical Minerals Prospectus highlights Tasmania's unique position in the world in hosting a diverse range of critical minerals alongside access to high-quality infrastructure and abundant renewable energy. A key objective of the Government's Critical Minerals Strategy is to grow exploration for these commodities.

To achieve this, Mineral Resources Tasmania is developing a series of prospectivity maps for critical mineral-bearing systems. These maps will promote investment, support exploration companies to target effectively, and provide strategic input into land use decision making. The maps will also be used to identify legacy drill core stored at the Mornington Core Library for resampling using modern analytical techniques to drive new discoveries across the state.

This study focussed on turbidite-hosted Au-Sb mineralisation in the northeast of the state. This region has produced a significant amount of gold, but modern exploration has been limited and the depth extent and the potential for the systems to host antimony may have been overlooked. Antimony is a critical mineral of increasing strategic importance, with primary applications in lead battery manufacturing, flame retardants, military applications, and the semiconductor industry. No antimony deposits are currently recorded in northeast Tasmania, however the prospectivity of the region warrants investigation considering correlations with analogous geological settings in Victoria, where economically significant antimony resources have been identified and mined, most notably at the Costerfield Au-Sb deposit east of Bendigo.

This study builds on previous work modelling granite-related tin-tungsten-fluorine-rubidium systems (Czertowicz, 2026) and forms part of a broader series of statewide critical mineral prospectivity mapping projects. All data and outputs produced from the study are included as a data package attached to this report (Appendices 1 and 2).

2.0 GEOLOGICAL SETTING AND TARGET MINERAL SYSTEM

2.1 Regional Setting

Tasmania comprises two distinct basement terranes referred to as Western and Eastern Tasmania (Baillie, 1985). The division between the terranes is obscured by Mesozoic sediments and associated dolerite intrusions, but is inferred to lie west of the Tamar Valley (Barton, 1999). Western Tasmania consists of Mesoproterozoic marine sedimentary successions and their deformed and metamorphosed equivalents, a Cambrian ophiolite allochthon, a post-collisional volcanic belt, Cambrian-to-Ordovician siliciclastic sequences, and Devonian granite intrusions (Berry et al., 2025). Eastern Tasmania is dominated by Ordovician deep-water turbiditic deposits intruded by voluminous granite batholiths. During the Middle Devonian, both terranes were deformed and likely sutured during the Tabberabberan Orogeny at *c.* 389 Ma (Black et al., 2005; Black et al., 2010).

The oldest rocks in northeast Tasmania belong to the Mathinna Supergroup, a sequence of Early Ordovician to Early Devonian turbiditic sandstones and mudstones (Figure 1; Banks and Baillie, 1989). Due to a scarcity of stratigraphic marker horizons and fossil age constraints, detailed subdivision of the unit has only been achieved in the region between the River Tamar and the Scottsdale Batholith (Seymour et al., 2011; Table 1). The Mathinna Supergroup is divided into the Ordovician Tippogoree Group and the Siluro-Devonian Panama Group, separated by an inferred fault that may be related to deformation associated with the Benambran Orogeny at *c.* 430 Ma (Reed, 2001). The following description is based on the stratigraphic framework of Seymour et al. (2011).

The basal unit of the Tippogoree Group is the Stony Head Sandstone, consisting predominantly of thick-bedded medium- to fine-grained quartz sandstone with minor pelitic interbeds. This unit is overlain by the Turquoise Bluff Slate, a sequence of massive to graded black slate containing minor siltstone beds.

Table 1. Latest stratigraphic subdivision of the Mathinna Supergroup (Seymour et al., 2011).

Supergroup	Group	Formation	Member	Age	Description
Mathinna Supergroup	Panama Group	Sideling Sandstone		Early Devonian	Fine-grained sandstone and interbedded siltstone
		Lone Star Siltstone		Late Silurian	Thin-bedded siltstone and interbedded fine-grained sandstone
		Retreat Formation		Silurian (?)	Interbedded medium to very fine-grained sandstone and siltstone-mudstone
		Yarrow Creek Mudstone		Silurian (?)	Thin-bedded mudstone and cross-laminated siltstone
	Tippogoree Group	Turquoise Bluff Slate		Early-Middle Ordovician	Phyllitic slate
			Industry Road Member	Early-Middle Ordovician (?)	Phyllitic slate and foliated very fine-grained sandstone
		Stony Head Sand-stone		Early Ordovician (?)	Fine-grained sandstone and minor pelite

At its base, the Turquoise Bluff Slate includes the Industry Road Member, characterised by interbedded phyllitic slate and very-fine-grained sandstone.

The base of the overlying Panama Group is defined by the Yarrow Creek Mudstone, comprising thin-bedded grey mudstone and minor quartz-siltstone and sandstone. This unit is conformably overlain by the Retreat Formation, which consists of interbedded medium- to fine-grained quartz sandstone with subordinate interbedded siltstone and mudstone. The Lone Star Siltstone conformably overlies the Retreat Formation and is characterised by thin-bedded plane-laminated siltstone, mudstone, and shale, with increasing sandstone beds toward the top of the formation. The uppermost unit of the Panama Group is the Sideling Sandstone, a succession of pale grey quartz sandstone with minor siltstone interbeds.

The Mathinna Supergroup preserves evidence of multiple phases of deformation, and a range of deformation histories have been proposed to account for the observed structures. The first event (D_1) involved east-directed thrusting, recumbent folding, and associated crustal thickening. Patison et al. (2001) assigned an Early Devonian age to this event, however Reed (2001) argued that D_1 affected only the two oldest units of the Mathinna Supergroup and proposed an Early Silurian age, correlating it with the Benambran Orogeny of mainland Australia.

The second event (D_2) occurred during the Devonian, prior to emplacement of Middle to Late Devonian granitoid plutons, and produced upright folds and cleavage with northwest vergence (Patison et al., 2001; Reed, 2001). Reed (2001) also identified a third event (D_3) which post-dated emplacement of predominantly I-type plutons but pre-dated most S-type intrusions. D_3 generated upright folds and southwest-vergent thrust faults. Overall crustal thickening associated with deformation resulted in lower greenschist facies metamorphism at a depth of *c*. 10 km (Patison et al., 2001).

The Mathinna Supergroup was intruded by numerous I- and S-type granitoids at *c*. 400-370 Ma (Figure 1; Corbett et al., 2014). These plutons include hornblende-biotite granodiorite, biotite granite, garnet-cordierite-biotite granite, and alkali-feldspar granite. Their emplacement broadly overlaps with the inferred timing of turbidite-hosted gold mineralisation in the region, suggesting that granite-related heat flow may have acted as a thermal driver for regional hydrothermal fluid circulation.

Younger units in northeast Tasmania include marginal portions of the Tasmanian Basin, comprising Permo-Triassic sedimentary rocks intruded by Jurassic dolerite, Tertiary gravel, and basalt, as well as Quaternary cover (Figure 1). Tertiary basalt is particularly widespread around the Pipers River, Scottsdale, and Derby areas.

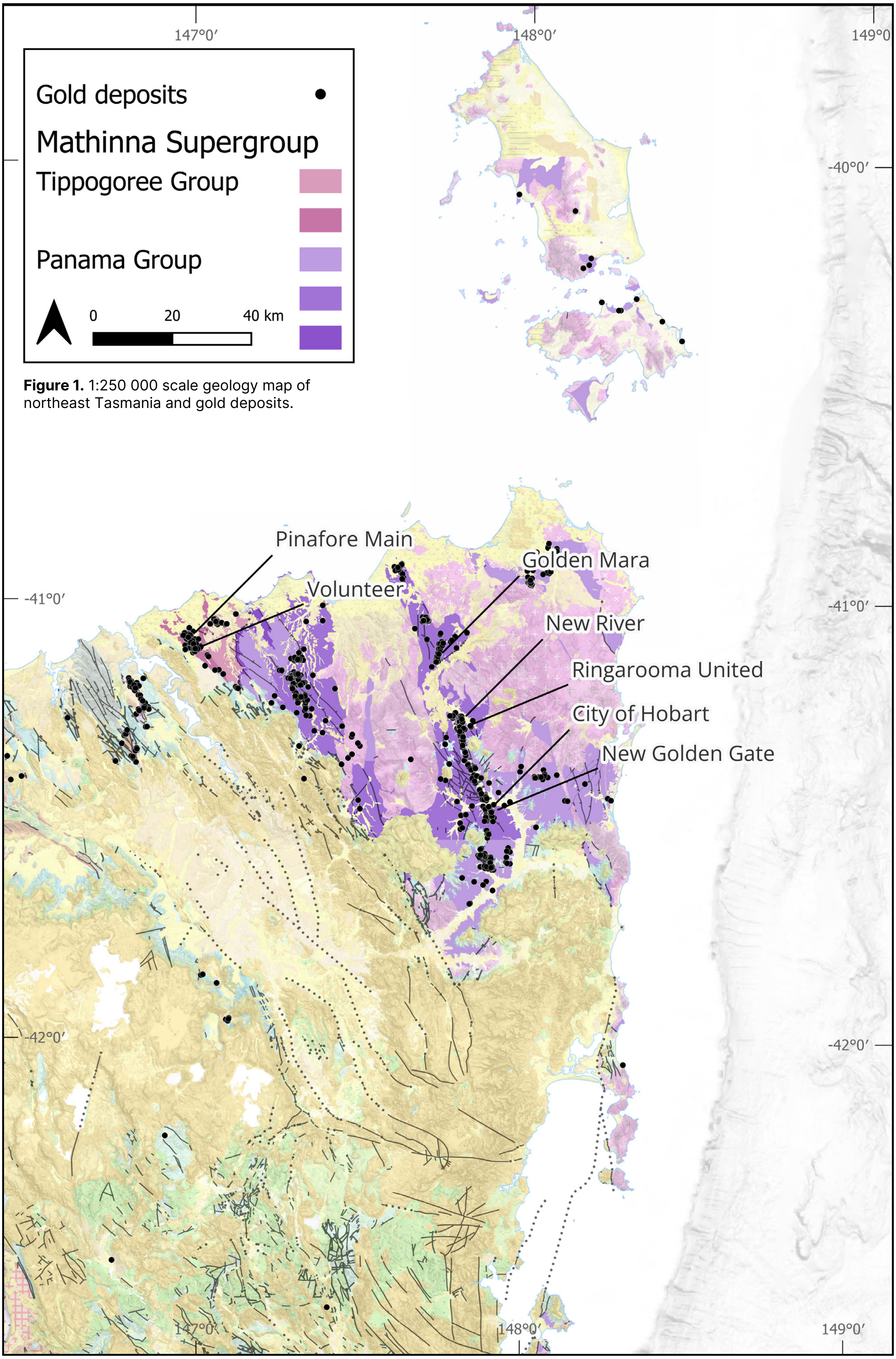

Figure 1. 1:250 000 scale geology map of northeast Tasmania and gold deposits.

2.2 Turbidite-hosted Au-Sb

Turbidite-hosted gold mineralisation is a subset of the orogenic gold deposit type. Orogenic gold deposits form in compressional settings, have a dominant structural control, and are deposited from low-salinity H_2O-CO_2 fluids at depths of 2-20 km (Groves et al., 2024; Kolb et al., 2015; Goldfarb et al., 2001; Groves, 1993). Turbidite-hosted gold deposits (also referred to as slate belt gold deposits) are defined as occurring within metasedimentary flysch packages, with lithological variations controlling the location and orientation of mineralised veins (Phillips and Hughes, 1998).

Turbidite-hosted gold mineralisation in northeast Tasmania was associated with Tabberabberan lower greenschist-facies metamorphism and deformation. The mineralisation is characterised by strong structural controls, fluids derived from metamorphic devolatilisation, and deposition in low-sulphide quartz veins. The turbidite-hosted gold deposits of northeast Tasmania have been correlated with slate belt deposits in Victoria due to similarities in host rocks, structural style, grade, and timing of mineralisation (Reed, 2004). The higher density and endowment of deposits in Victoria indicates that significant undiscovered resources may remain in northeast Tasmania.

As well as gold, these systems are considered prospective for antimony. This potential is difficult to determine due to incomplete historical reporting and a lack of assays, however the presence of large Au-Sb deposits in analogous settings in Victoria such as Costerfield indicates that the antimony potential of the region warrants further investigation.

In the northeast Tasmania systems, gold is hosted within Mathinna Supergroup rocks, typically proximal to transitions between sandy and silty facies where ductility contrasts result in dilation and a favourable environment for mineralisation (Figure 1; Reed, 2004). Gold deposition was likely triggered by pressure drops associated with dilation and by redox reactions with carbonaceous host rocks (Taheri, 1993). Gold occurs in dominantly NNW- and less commonly NE-trending quartz veins, typically laminated and grey, and containing minor pyrite, arsenopyrite, chalcopyrite, sphalerite, and galena. The veins are up to 2 km long and 7 m wide but exhibit local geometric complexities that result in complex grade distributions. Little to no alteration surrounds the deposits, except for a report of silicification around the Golden Gate mine (Reed, 2004).

Mineralising fluids have been found to be H_2O-CO_2 fluids with an inferred metamorphic origin (Bottrill et al., 1992). However, in the Mangana-Forester area, Taheri and Bottrill (1995) identified both metamorphic fluids and a minor CO_2-poor, low-temperature fluid similar to greisen-related fluids, indicating that minor remobilisation of gold by granite-related fluids had occurred locally. Gold is inferred to have been sourced from devolatilisation of basalt, ultramafics (inferred to occur at depth in the region, e.g. Roach, 1994), or greywackes during greenschist to amphibolite grade metamorphism (Bottrill et al., 1992).

Important structural controls for turbidite-hosted Au-Sb mineralisation in northeast Tasmania include shear zones, strike-slip faults, anticlinal crests and limbs, cross folds, and extensional jogs, with most gold associated with D_3 compression (Reed, 2004). Ductility contrasts between sandy and silty facies controlled fault and fold geometries and therefore the localisation of gold mineralisation (Corbett et al., 2014).

The timing of gold mineralisation has been constrained by Ar-Ar dating, with most ore formation inferred to have occurred in the Middle Devonian between 395 and 385 Ma, which is consistent with the timing of peak deformation during the Tabberabberan Orogeny (Bierlein et al., 2005). Less common older ages of 420-430 Ma are recorded in alteration halos and indicate an earlier Silurian phase of deformation and mineralisation.

The relationship between turbidite-hosted gold deposits and Devonian granites is unclear. Roach (1992) found that in the Alberton-Mangana goldfield, deposits were underlain by granite at depth and that granodiorites occurred in the vicinity of mineralisation, but a causal relationship could not be established. Taheri and Bottrill (2005) suggested that the distribution of gold deposits at Mathinna may be spatially associated with a thermal aureole around the Pyengana Granodiorite.

In addition to the turbidite-hosted deposits, intrusion-related gold deposits also occur in northeast Tasmania, and there may be overlap or overprinting between these two distinct styles. The intrusion-related deposits are typically hosted in aureoles around granitoids but can occur within the intrusions themselves and are thought to have been coeval with the turbidite-hosted systems (Figure 1; Bierlein et al., 2005). Intrusion-related deposits typically contain more base metals and elevated Ag, As, Sb, W, and Bi compared to turbidite-hosted deposits, although the scarcity of whole-rock geochemistry data makes this distinction problematic for a number of deposits. This study focuses on turbidite-hosted systems only; however, the potential for overlap between these systems was considered throughout the modelling.

Total gold production in the northeast is reported as 19.8 tonnes (636 585 oz), 23 % of which was mined from alluvial sources, however due to incomplete record-keeping, true production figures were likely much higher and have been estimated at 29.7 tonnes (954 877 oz) (Bottrill, 1991). Significant turbidite-hosted gold deposits in northeast Tasmania are listed in Table 2.

Defined resources include an Inferred Resource for New Golden Gate of 42,196 tonnes @ 10 g/t Au (Holden, 2010), and an exploration target of 3.5-5.4 Mt @ 3.0 to 4.0 g/t Au for Flynn Gold's Golden Ridge Project (Flynn Gold, 2024a).

The most significant region for gold production was the 70 x 6 km NNW-trending Mathinna-Alberton Gold Lineament, located between the Scottsdale and Blue Tier batholiths (Bottrill et al., 1992). This region includes the largest deposit in the province, the New Golden Gate mine, which has a reported production of 7197 kg at 25 g/t Au. Within the lineament, gold occurs in NNE and NE-trending quartz veins with minor carbonate, sericite, arsenopyrite, pyrite, and base metal sulphides, hosted in faults and silicified shear zones (Roach, 1992). The primary control on the goldfield is thought to be a regional dextral strike-slip fault, with gold deposition occurring in dilational jogs (Roach, 1992).

3.0 METHODS

3.1 Mineral Potential Mapping

Mineral potential mapping aims to use available geoscientific data to predict the likelihood of discovering a mineral deposit at a given location. All methods essentially combine the input datasets using an algorithm to produce an output heatmap showing the relative prospectivity over a study area. The simplest approach is to use a knowledge-driven method, such as fuzzy logic, where data layers known to map critical components of the mineral system (referred to as predictor maps) are overlain and weighted according to their importance. Data-driven methods are favoured in well-explored regions and use known examples of mineralisation (commonly deposit locations) to train the model, essentially determining the weights for each input based on the spatial correlation between the deposit training points and the predictor layer. Examples of data-driven methods include weights of evidence, logistic regression, and machine learning techniques such as random forest, support vector machines, and gradient boosting machines. This study used an ensemble random forest method, described in further detail below.

Table 2. Significant historical gold mines in northeast Tasmania.

Deposit	Goldfield	Total Recorded Gold Production
New Golden Gate	Mathinna	7197 kg
Pinafore	Lefroy	1712 kg
Volunteer	Lefroy	1277 kg
City of Hobart	Mathinna	596 kg
Ringarooma United	Alberton	255 kg
New River	Alberton	131 kg
Golden Mara	Mt Horror	104 kg

3.2 Mineral Systems Approach

A mineral system refers to the large-scale focussing of energy and mass flux in the crust, which results in the formation of mineral deposits (Wyborn et al., 1994). Deposit formation is dependent on deriving ore-forming components from a source, transporting and accumulating the components in a trap, depositing metals, and preserving the metals through geological time. If any of these processes are lacking, no deposit will form.

As well as metals, a source needs to provide heat, energy, and fluids, which are required to mobilise the metals. Various fluid pathways can be involved in transportation of the ore-bearing fluid including faults, shear zones, and porous rocks. Traps may be chemical, involving reactive host rocks that reduce the solubility of the metals, or physical, which typically involve focussing of large volumes of fluid through a restricted region of the crust.

The mineral system approach is particularly well-suited to mineral potential mapping since each of these critical processes can be mapped using geological proxies. It also captures the inherent variability within deposit classes, allowing a range of styles to be targeted in a single model.

3.3 Modelling Workflow

The modelling for this study was conducted over the northeast of Tasmania at a resolution of 40 m. This resolution was chosen to match the magnetic dataset, as this represents the highest resolution geophysical input data used in the modelling. Using the finest resolution ensures that the model captures the most spatial detail possible, preserving small-scale variations which may reflect key expressions of the target mineral system. Advances in computing hardware and machine learning algorithms allow models covering large areas to be run at high spatial resolution within practical timeframes. The study area for this project was selected to include all parts of eastern Tasmania with outcropping Mathinna Supergroup rocks, including the Furneaux Islands, Freycinet Peninsula, and Maria Island.

The workflow used for the prospectivity mapping was built on that used for granite-related tin-tungsten-fluorine-rubidium systems (Czertowicz, 2026) and involved the following major steps:

1. Review of the mineral system and determination of important predictor maps
2. Compilation and validation of relevant geological, geophysical, and geochemical datasets
3. Selection and weighting of training points
4. Preparation of predictor maps using GIS methods
5. Modelling using a Random Forest ensemble to produce output prospectivity and uncertainty maps
6. Validation of the results.

The final two steps were iterated to produce the most geologically reasonable and practically useful output.

Datasets used for the modelling were sourced from Mineral Resources Tasmania and Geoscience Australia and included 1:250 000 geology mapping (including folds, faults, contacts, and unit polygons); several geophysical datasets including a DEM, gravity, magnetics, magnetotellurics, and radiometrics; as well as rock chip, stream sediment, drillhole, observations, and mineral occurrence databases (Table 3).

Quality assurance and quality control (QA/QC) procedures were undertaken on all input data prior to modelling, which included verification of spatial alignment and coordinate systems in GIS, validation of geometries, review of geological attributes, and removal of duplicates and invalid geochemical values. All input data were standardised to a common model grid and coordinate system (GDA1994 zone 55) to ensure pixel locations matched exactly. Following this, additional attributes were compiled, and numerous processing approaches were used to generate predictor maps, including buffering, density calculations, worm extraction from magnetic and gravity data, and terrain texture analysis.

Table 3. Datasets used for the modelling.

Dataset	Source	Download Link
1:250 000 Geology (polygons, faults, contacts, linears)	Mineral Resources Tasmania	https://www.mrt.tas.gov.au/products/digital_data/data_downloads/geology_of_tasmania
Mineral Occurrences	Mineral Resources Tasmania	https://www.mrt.tas.gov.au/products/digital_data/data_downloads/mineral_occurrences_data
Mineral Drillholes	TIGER database	https://www.mrt.tas.gov.au/products/digital_data/data_downloads/boreholes_drill_holes_data
Samples and observations	TIGER database	https://www.mrt.tas.gov.au/products/digital_data/data_downloads/samples_and_observations_data
Magnetotellurics	AusLAMP	https://ecat.ga.gov.au/geonetwork/srv/eng/catalog.search#/metadata/149489
Magnetics	Mineral Resources Tasmania	https://www.mrt.tas.gov.au/products/digital_data/data_downloads/geophysics_data
Gravity	Mineral Resources Tasmania	https://www.mrt.tas.gov.au/products/digital_data/data_downloads/geophysics_data
Radiometrics	Mineral Resources Tasmania	https://www.mrt.tas.gov.au/products/digital_data/data_downloads/geophysics_data
DEM	Mineral Resources Tasmania	N/A
Modelled Devonian granite upper surface	Mineral Resources Tasmania	N/A (after Leaman and Richardson, 2003; Leaman, 2012)

3.4 Training Data

Known hard-rock gold deposits with historic resources or production figures were used as positive training points for the modelling (Table 4). A total of 40 deposit locations were extracted from the mineral occurrence database. Deposits were reviewed by a domain expert (Ralph Bottrill) to ensure that they accurately represent the target mineral system. An attempt was made to exclude intrusion-related gold deposits through manual review of the dataset. Deposits located within or immediately adjacent to granitoid intrusions, as well those with anomalous tungsten or bismuth signatures, were removed. However, because the two gold deposit styles can overlap and overprint one another, it is likely that some intrusion-related deposits remain in the training set. Nevertheless, given the large number of training points and the greater weighting assigned to larger, better-characterised deposits, the influence of any remaining intrusion-related deposits on the model is expected to be minimal.

Any deposits attributed in the database with a location error of greater than 500 m were removed, as well as any deposits within 500 m of another deposit, prioritising the larger deposits.

Training data were weighted to ensure that the largest deposits have greatest influence over the model, since larger deposits are better understood and represent the primary targets for explorers. Gold production figures were compiled for the training data, and ten quantiles were created and used to generate weights ranging from 1 to 10, representing deposits with no recorded production up to the largest deposits.

A common challenge in machine learning-based prospectivity mapping involves the selection of negative training points. Ideally, these points should represent locations where mineralisation related to the target mineral system is known to be absent. In practice, such data are rare and therefore proxy negative datasets are typically used. These include mineral occurrences related to other mineral systems (Nykanen et al., 2015), locations within non-permissive geology (Ford, 2020; Kreuzer and Roshanravan, 2025), and randomly generated points (Carranza and Laborte, 2015). Barren drillholes have also been proposed as a source of negative training data due to their direct sampling of the target geological environment, although their application in published studies is limited. However, drillhole locations are themselves spatially biased toward areas considered prospective, and may still occur proximal to, or directly within, mineralised zones, meaning that “barren” intersections do not necessarily represent true absence of mineralisation. Due to the availability of data,

Table 4. Positive training data used in the modelling.

Name	Locality	Gold Production (Kg)	Weight
New Golden Gate	Mathinna	7197	10
Pinafore Main	North Of Lefroy	1712	10
Volunteer	South Of Lefroy	1277	10
City of Hobart	Mathinna	596	10
Ringarooma United	Alberton	255	10
New River	Alberton	131	9
Golden Mara	Warrentinna	104	9
Golden Entrance No. 1 Shaft	Napkin Hill	91	9
Volunteer Mine	Mathinna	73	9
Golden Crown	Lefroy	60	8
Buckland	Bucklands Hill	36	8
Volunteer Consolidated	Mathinna	36	8
Linton P.A.	Between Williams and Trig Hill	30	8
New Eldorado	Mathinna	26	7
Miami	Nw Of Mathinna	20	7
Una	Mt Victoria	15	7
Fingal	Grants Creek, Union Jack	9.9	7
Cardinal	Bucklands Hill	4.9	6
Portland	Gladstone	2.9	6
Crown Prince	Alberton	2.7	6
Caxton No. 1	Alberton - Mt Victoria	2.4	5
Leura	East Of Back Creek	2.4	5
Jubilee Gold Mine	Mathinna	1.7	5
Horseshoe	Mathinna	1.4	5
Scott and Pickett	Mathinna	1.1	4
Great Fingal	N Bank, Little Hospital Creek	1.0	4
Enterprise	Mathinna	0.93	4
Frog	Alberton	0.93	4
Pincher	Mangana	0.31	4
West Miami	Mullens Creek Tributary	0.23	3
Abbotsford Creek	South Esk River	0.22	3
Dawn of Peace	Warrentinna	0.19	3
Sunbeam Reef	E Of Tower Hill	0.12	2
Alliance	Lyndhurst	0	1
Apple Orchard Point	North Coast, Cape Barren Island	0	1
Browns Reef	Long Point	0	1
McCauls	Alberton	0	1
Never Mind	Back Ck, S of Turquoise Bluff	0	1
New Land O'Cakes	South Of Lefroy	0	1
Victorian Golden Gate	Mathinna	0	1

the regional scale of the modelling, and the need to avoid bias, randomly generated negative training points were used in this study. These points were generated outside of a 1 km exclusion zone around positive training points to avoid placing negative points inside potentially prospective ground. The number of negative training points generated was equal to the number of positive points. The negative points were assigned a weight of 1 and the weights of the positive training points were normalised to ensure balance between the sum of positive and negative weights. This 1:1 ratio was selected to address class imbalance, which is often present in mineral potential mapping due to deposits representing relatively rare features.

Multiple sets of negative training data were tested with the same model parameters and input maps to determine the sensitivity of the models to the selection of negative training points. The results, while highlighting the same broad prospective zones, had significant differences, particularly in areas of moderate prospectivity. Therefore, instead of relying on a single set of negative training points, ten random sets were generated per model, resulting in ten distinct prospectivity maps, which were then averaged to produce the final output. This ensemble approach smooths out the effects of negative training point selection to produce a more reliable and reproducible result. The ensemble modelling method also has the benefit of producing a standard deviation map from the multiple model runs, indicating where the selection of different negative training datasets had the largest effect on predicated prospectivity.

3.5 Predictor Maps

The mineral system approach was used to define 135 predictor maps representing proxies for the key components (Table 5, Figure 2). Each map represents either a source, transport, trap, or deposition process that may have occurred during mineralisation. Since orogenic gold deposits form distal from their metal source, only limited source maps were integrated into the models.

These maps were tested in various iterations of the modelling, with the most effective and geologically reasonable predictors retained in the final models. Known predictors of regional-scale turbidite-hosted Au-Sb mineralisation in Tasmania that informed predictor map generation included Mathinna Supergroup rocks, point observations of carbonaceous rocks, rheological contrasts, minor faults, fault density, fault intersections, quartz veins and anomalous Au, As, Sb geochemistry. Many other diverse predictive maps were generated and tested to determine predictive capability.

Table 5. Predictor maps incorporated into the modelling and corresponding mineral system components.

<table>
<tr><th colspan="4">Turbidite-hosted Au-Sb</th></tr>
<tr>
<td>Source:
Magnetotelluric depth slices
Gravity (residual, Bouguer, textural derivatives)
Granodiorite</td>
<td>Transport:
Faults (types, orientations, size)
Fault intersections
Fault rock observations
Geological contacts
Magnetics (RTP, 1VD, tilt, upward continuations, textural derivatives)
Gravity and magnetic worms
DEM (including slope and textural derivatives)</td>
<td>Trap:
Mathinna Supergroup
Competency contrasts
Folds
Carbonaceous rocks
Magnetic anomalies
Fault intersections
Fault density
Radiometrics</td>
<td>Deposition:
Vein/sulphide observations
Geochemical anomalies
Placer gold occurrences</td>
</tr>
</table>

Figure 2. Example predictor maps used as inputs for the random forest modelling.

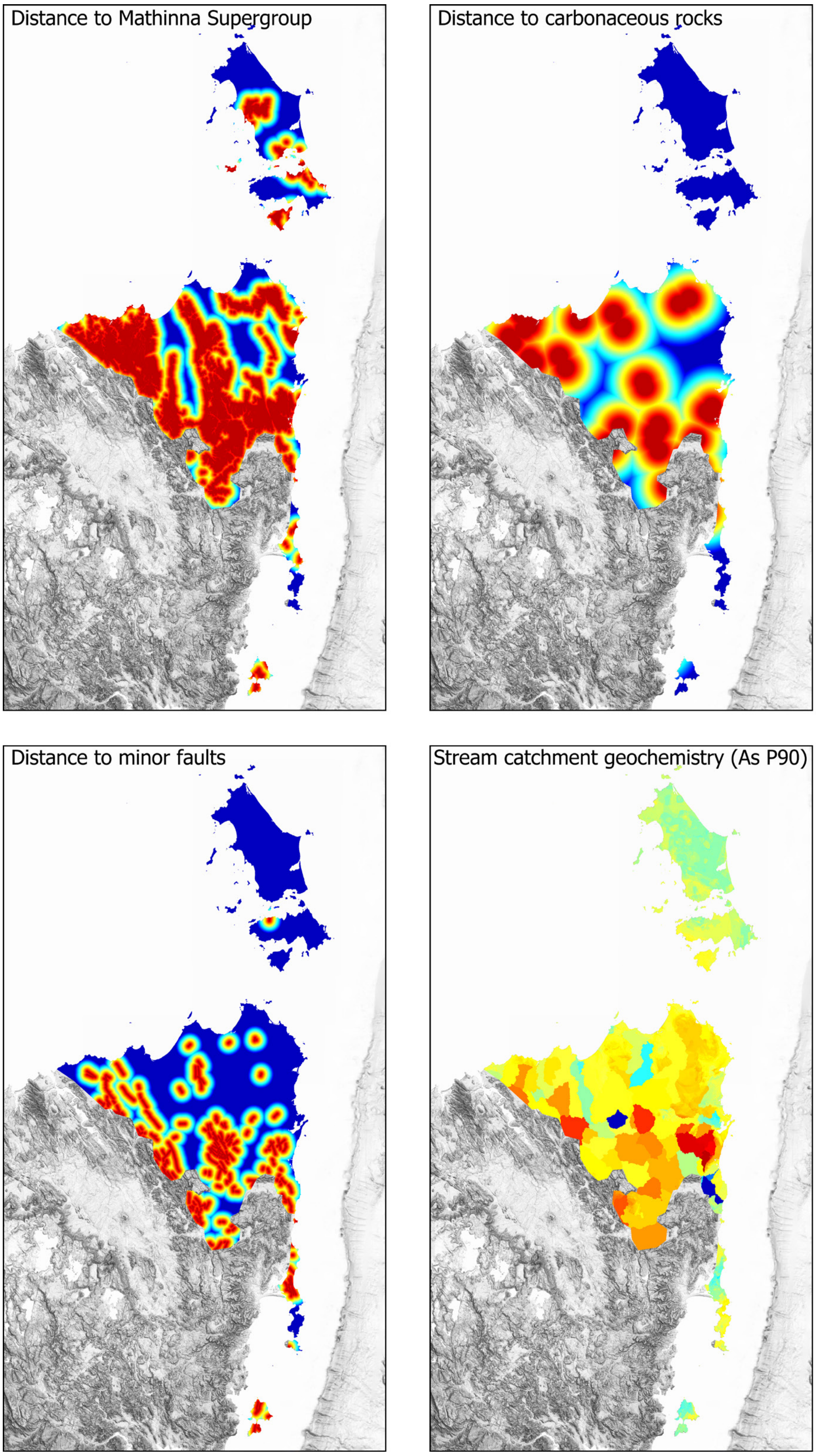

Some datasets required minimal processing and could be used directly, such as certain gravity and magnetic grids. Derivatives of geophysical data generated included upward and downward continuations and worm analysis to enhance horizontal gradients.

Proximity-based predictor maps were created by buffering datasets including faults, source rocks, and rock chip anomalies. Queries were commonly applied to source datasets prior to buffering to isolate specific features of interest (e.g., orientations of faults, carbonaceous rocks). A density map was also created from the fault dataset to quantify deformation intensity.

Geochemical statistics were analysed using the ioGAS software package. Threshold values for the rock chip maps were selected using a combination of probability plots and consideration of percentiles. Stream sediment data were assigned to catchments using percentiles, median, and maximum statistics on log-transformed data.

Texture analysis of geophysical datasets was performed using the Gray-level Co-occurrence Matrix (GLCM) method. This analysis compares pixel values within a chosen search window and provides metrics such as contrast and entropy that characterise textural variations in the data.

3.6 Random Forest

Random forest (Breiman, 2001) is a machine learning algorithm that has been successfully applied to mineral potential mapping applications in various settings (Carranza and Laborte, 2015; Ford, 2020; Zhang et al., 2022; Kreuzer and Roshanravan, 2025). It is particularly well suited to geological applications due to its ability to handle sparse training data, spatially correlated and missing data, as well as its computational efficiency and reproducibility. Random forest also outputs measures of variable importance, indicating which maps contributed most to the classification.

This allows assessment of whether the model is operating in a geologically reasonable manner by highlighting which inputs are driving the predictions. Decision tree thresholds can also be extracted and analysed to confirm that they are geologically meaningful. This interpretability contrasts with "black box" approaches such as deep neural networks, where such insights can be difficult or impossible to obtain.

Random forest implementation occurs in two stages: training and classification. During training, known mineral deposits and nominal non-deposit locations are used to learn which combinations of input maps best discriminate deposits from non-deposits. The algorithm generates multiple decision trees; each built from a random subset of predictor maps and a bootstrapped sample of training data. Each node in a tree applies a threshold (e.g., distance or geochemical concentration) to a specific predictor map, chosen to optimize separation between deposits and non-deposits (Figure 3). The final classification for each pixel is determined by majority vote across all trees in the forest. During the classification stage, the trained forest is applied over the entire study area. Rather than producing a binary prospectivity map, the more commonly used output in geological applications is a probability map, where values range from 0 to 1 and represent the proportion of trees that classified each pixel as prospective.

3.7 Random Forest Implementation

In this study, random forest was implemented using the scikit-learn library in Python, while QGIS was used for spatial pre-processing and visualisation of results. Hyperparameters were tuned through iterative manual testing to optimise model performance, balancing efficiency with accuracy. The final configuration was:

- Number of trees (n_estimators): 500
- Maximum tree depth (max_depth): 15
- Maximum number of features per split: square root of total
- Minimum samples per leaf (min_samples_leaf): 5
- Minimum samples per split (min_samples_split): 10

Missing values in the predictor maps were imputed using a separate random forest model trained on the available data, which uses the relationships between predictor maps to estimate values where data are absent. Imputation results were visually reviewed to verify that the results were geologically reasonable.

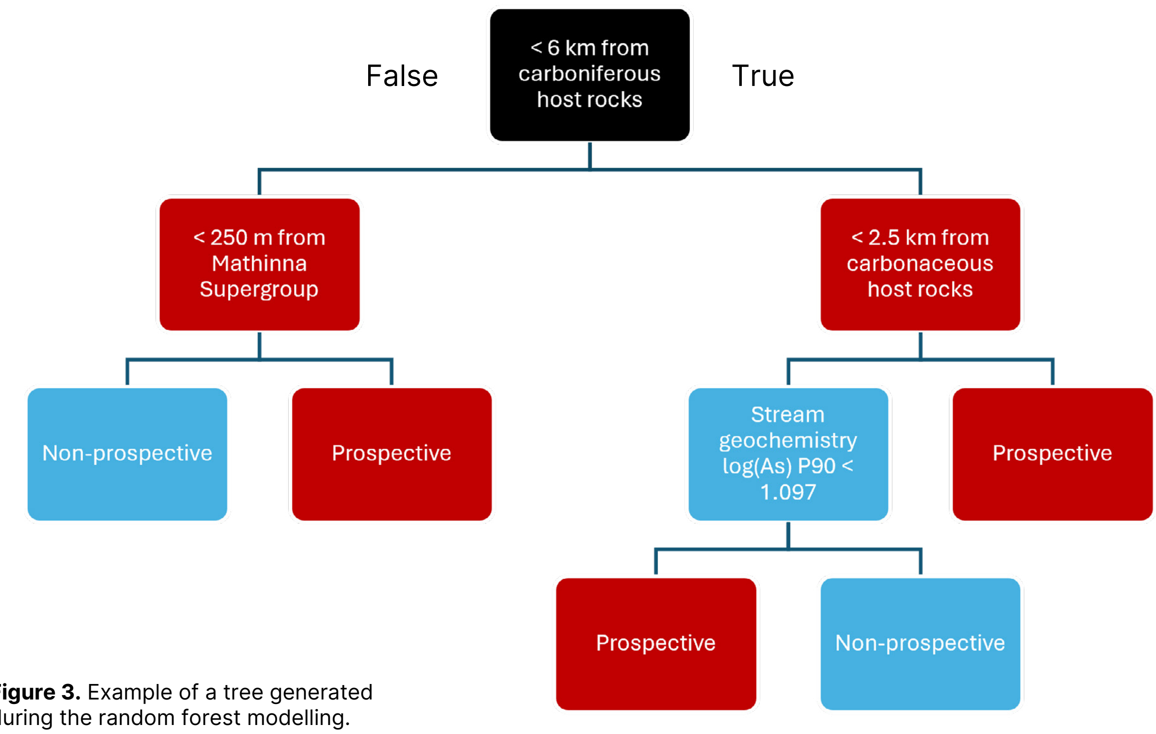

Figure 3. Example of a tree generated during the random forest modelling.

An ensemble random forest approach was developed whereby several random forest models were trained using different sets of randomly generated negative points. The resulting prospectivity predictions were combined to produce mean and standard deviation maps representing the overall prospectivity and the uncertainty associated with negative training point selection, respectively. Testing indicated that model outputs and uncertainties converged to a satisfactory level after approximately eight forests. To ensure robust results while maintaining computational efficiency, a standard ensemble of 10 forests was adopted.

3.8 Validation

Several validation metrics were generated to assess model performance. These included out-of-bag (OOB) error, k-fold cross-validation, receiver operating characteristic, and success rate curves.

Out-of-bag error is calculated using training data not included in the bootstrapped sample used during tree generation, providing an internal test of model accuracy.

Cross-validation repeatedly splits the training data into different subsets, training the model on one portion and testing it on the remaining, unseen points. In this study, five folds were generated, and a separate test was run using each set of negative training points with the results averaged. It should be noted that the resulting scores will be an overestimate of true model accuracy due to the tendency for variables to be more similar to each other at nearby locations. Ideally, cross validation folds are generated in spatial blocks, however, this was not practical for this project due to the limited number and concentrated distribution of positive training points.

Receiver operating characteristic curves (Nykanen et al., 2015) plot the model's true positive rate against its false positive rate across the range of prospectivity values. The area under the curve (AUC) summarises the performance, where 1 indicates perfect discrimination and 0.5 is no better than random choice.

Success rate curves show the cumulative percentage of known deposits captured as a function of the percentage of the study area, starting from the most prospective areas and moving out, reflecting the model's spatial efficiency. The AUC provides a metric for comparing model performance, with higher values indicating better discrimination between prospective and non-prospective ground.

Further validation of the models was conducted via expert geological feedback during meetings held at Mineral Resources Tasmania with Ralph Bottrill, Mike Vicary, John Everard, and Mark Duffett. Model predictions were compared to the current understanding of the mineral system, and any discrepancies were discussed and addressed in subsequent model iterations. This approach ensured that expert geological knowledge was systematically incorporated into the data-driven model, aligning the model result with established geological understanding of the mineral system.

4.0 RESULTS

A total of 31 models were run during an iterative development process, with two selected as the final output products. These comprise one model using only geophysical data inputs (Model 1) and another using maps derived from all data types (Model 2). The goal of this two-model approach was to investigate the difference in output using only objective, continuous, and quantitative geophysical data versus including geological and geochemical maps which may contain biases related to mapping coverage, sampling density, or geological interpretations, but that nevertheless improve the predictive capacity of the model.

A list of predictor maps included in the two models is provided in Table 6. The selection of maps was based on their relevance to the mineral system, performance in previous model iterations, and their ability to capture unique map patterns.

Variable importance scores, which indicate the contribution of each predictor to the models, were computed for each model (Table 6; Figures 4 and 5). These scores were calculated using Gini importance, which quantifies the total reduction in node impurity (i.e. improvement in the separation of prospective and non-prospective classes) attributed to each predictor across all decision trees in the random forest. Higher scores therefore indicate predictors that more effectively differentiate between prospective and non-prospective areas.

For Model 1 (geophysics-only), highest importance scores were recorded for radiometric maps (particularly Th and Th/U) and a gravity worm density map. All other maps had moderate contributions to the model. Figure 4 also shows the standard deviation of the importance scores, showing how the scores varied as negative training sets were changed. The Th/U map has a small standard deviation indicating that it was a useful discriminator across all model runs.

Model 2 (comprehensive) is largely dominated by maps showing carbonaceous rocks, fault rocks, and Mathinna Supergroup rocks (Figure 5). The highest ranked geochemistry map was copper in stream catchments, although arsenic and gold had similar scores. Moderate scores were attributed to minor faults, competency contrasts, and fault density maps. Radiometric Th/U was again the strongest geophysical predictor.

Table 6. Predictor maps used in the final two models. Variable importance indicates the contribution of each map to the result and sums to one.

Predictor Map	**Variable Importance Model 1**	**Variable Importance Model 2**
GEOPHYSICS		
Magnetics - RTP	0.05	0.01
Magnetics - upward continuation (689 m)	0.04	0.01
Magnetics - contrast texture filter	0.05	0.02
Magnetics - energy texture filter	0.08	0.02
Magnetics - entropy texture filter	0.07	0.02
Magnetics - homogeneity texture filter	0.07	0.02
Gravity - residual	0.07	0.02
Gravity - residual - worm density (1165 m)	0.11	0.02
Radiometrics - Th	0.12	0.02
Radiometrics - Th/U[MD1.1][TC1.2]	0.17	0.04
Radiometrics - K/Th	0.04	0.01
DEM	0.07	0.02
DEM - energy texture filter	0.06	0.01
GEOLOGY		
Proximity to Mathinna Supergroup rocks		0.12
Proximity to competency contrasts		0.05
Proximity to carbonaceous rocks		0.19
Proximity to minor faults		0.05
Proximity to fault intersections		0.01
Fault density		0.04
Proximity to fault rock observations		0.16
GEOCHEMISTRY		
Stream geochemistry - Ag		0.01
Stream geochemistry - As		0.04
Stream geochemistry - Au		0.04
Stream geochemistry - Cu		0.06

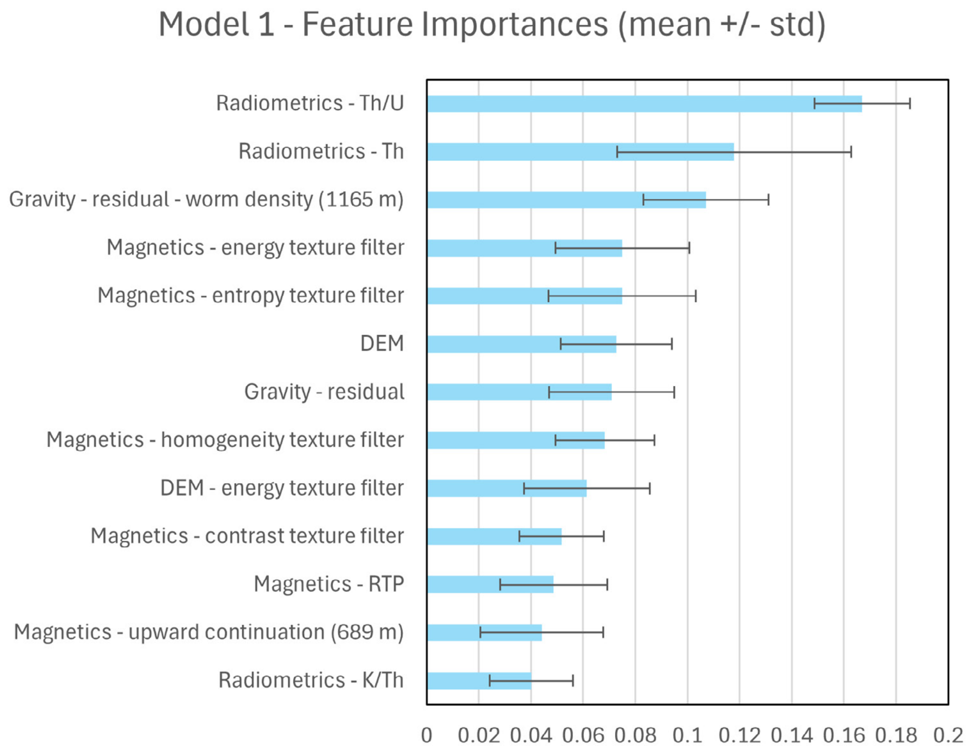

Figure 4. Variable importance scores for predictor maps used in Model 1.

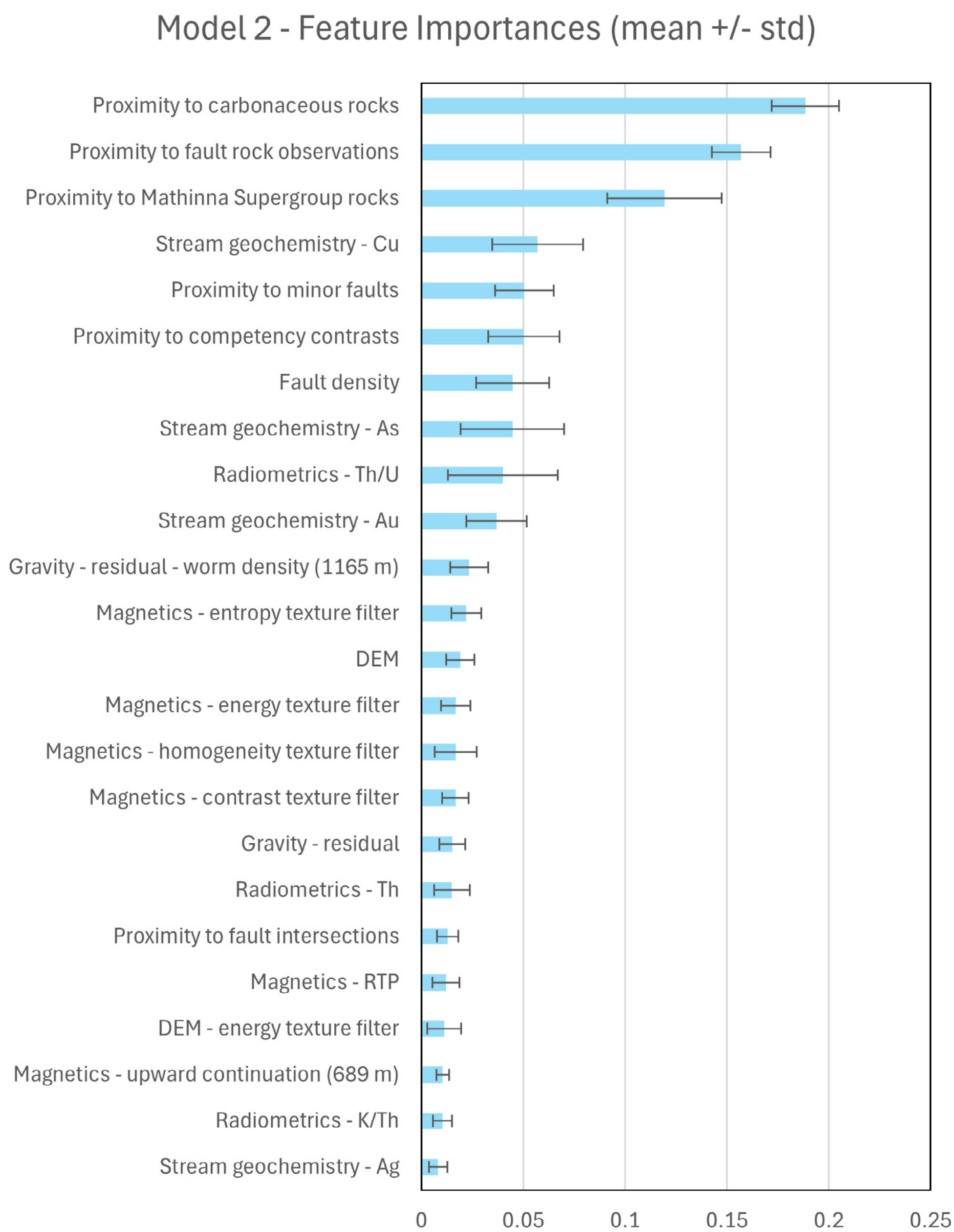

Figure 5. Variable importance scores for predictor maps used in Model 2.

Partial dependence plots for the top eight variables from Model 2 are shown in Figure 6. These plots illustrate the change in prospectivity score ascribed to variation in each predictor, with all other predictors held constant. Deciles indicating the locations of positive and negative training data are shown as rug plots at the base of each figure. Variables with plateaus separated by steep gradients, such as distance to carbonaceous rocks, are strong predictors that effectively separate prospective and non-prospective training data. In contrast, variables with gentle gradients are less discriminatory.

4.1 Performance Metrics

Model performance metrics are summarised in Table 7. Both models display strong overall performance, but Model 2, which includes more diverse predictor maps, consistently outperforms Model 1 across all metrics. This shows that while a geophysics-only approach is effective, the addition of geology and geochemical maps significantly improves

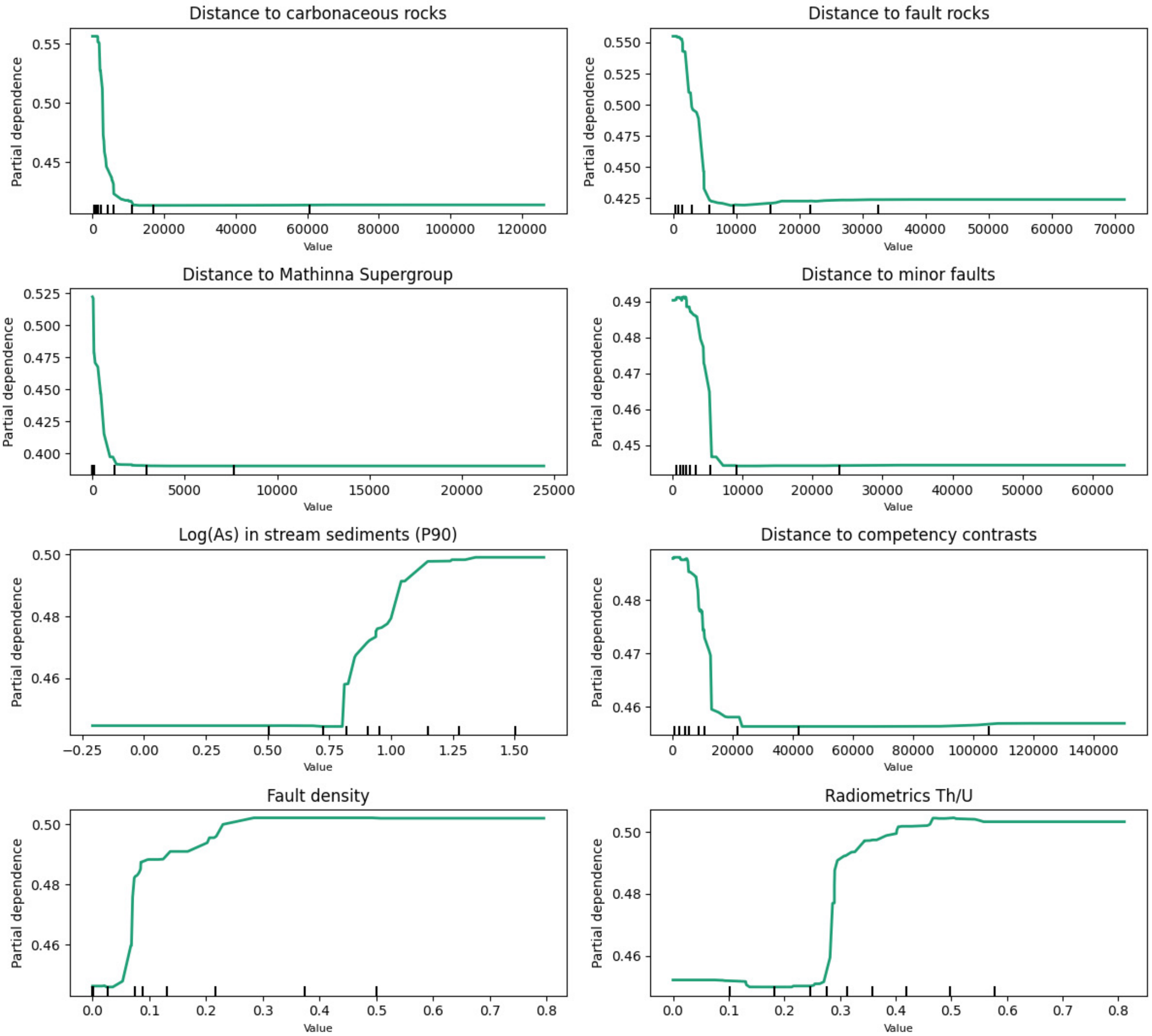

Figure 6. Partial dependence plots for the top eight variables from Model 2.

Table 7. Performance metrics for the two ensemble models. Results of a standard random forest are included for comparison with Model 2.

	Model 1	**Model 2**	**Model 2 (standard random forest)**
Out-of-bag Score	0.81 ± 0.02	0.87 ± 0.02	0.84
Cross Validation Score	0.79 ± 0.10	0.84 ± 0.08	0.83
ROC score	0.98	0.99	0.98
Success Score (training)	0.92	0.96	0.96
Success Score (validation)	0.87	0.96	0.95

predictive capability. To evaluate the benefit of the ensemble approach, Model 2 was also run as a standard random forest using a single set of randomly generated negative training points (Table 7). The ensemble method produced modest but consistent improvements across all performance metrics, suggesting that averaging across multiple negative training datasets improves model robustness.

Both models achieved high out-of-bag (OOB) and cross validation (CV) scores, with a notable improvement in both metrics for Model 2. The decrease from OOB to CV performance is expected as OOB scores are generally optimistic relative to CV, since out-of-bag samples are excluded from individual trees but may still be represented elsewhere in the ensemble. Model 2 shows lower variance in CV scores, indicating more stable performance across different training subsets.

As mentioned in section 3.8, CV scores are likely inflated by spatial autocorrelation within the training data. Nevertheless, they remain useful for comparing models, and the relative improvement from Model 1 to Model 2 is considered meaningful. ROC AUC values are high for both models, confirming strong discriminatory performance, with a marginal improvement for Model 2.

Success rate curves (Figure 7) measure the proportion of known deposits captured within progressively smaller areas of predicted high prospectivity. Performance was evaluated using both the positive training dataset and an independent validation dataset comprising gold deposits not used during model training. Although these validation deposits were selected to represent turbidite-hosted deposits, many are small and poorly characterised, and may not represent genuine turbidite-hosted mineralisation. Despite these uncertainties, both training and validation success rates improve from Model 1 to Model 2. The difference between training and validation scores decreases from 0.05 to 0, suggesting that Model 2 generalises well to unseen data and is less affected by overfitting.

Model 1 captures 90 % of the known deposits within 17 % of the study area, while Model 2 captures 95 % of the known deposits within only 12 % of the area. Both models therefore demonstrate strong exploration efficiency,

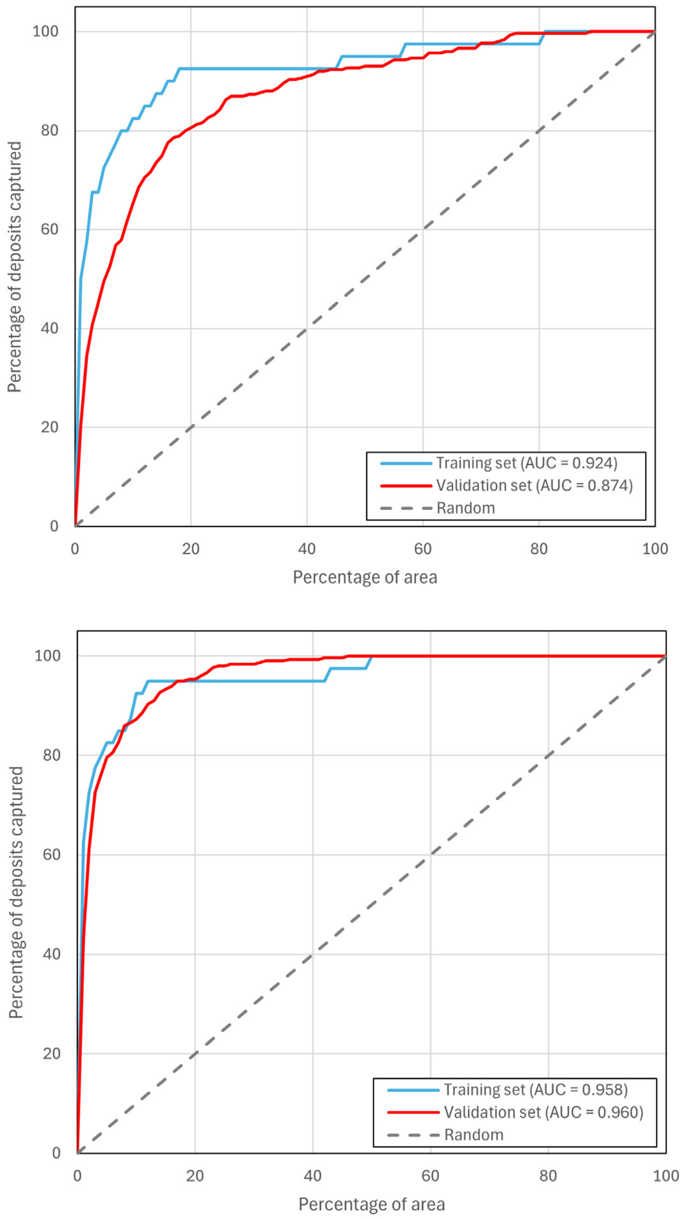

Figure 7. Success rate curves for the two models.

providing a significant reduction in exploration search space.

4.2 Output maps

Output mineral potential maps are shown in Figures 8 and 9. These probability maps show the relative prospectivity for turbidite-hosted Au-Sb mineralisation across northeast Tasmania. Scores range from 0 to 1, representing the proportion of trees that voted for the prospective class, and therefore the results are best used as relative rankings of prospectivity across the study area rather than absolute probabilities of finding a deposit. Almost all known turbidite-hosted gold deposits plot within the highly prospective areas, validating the models' ability to capture sites of known mineralisation.

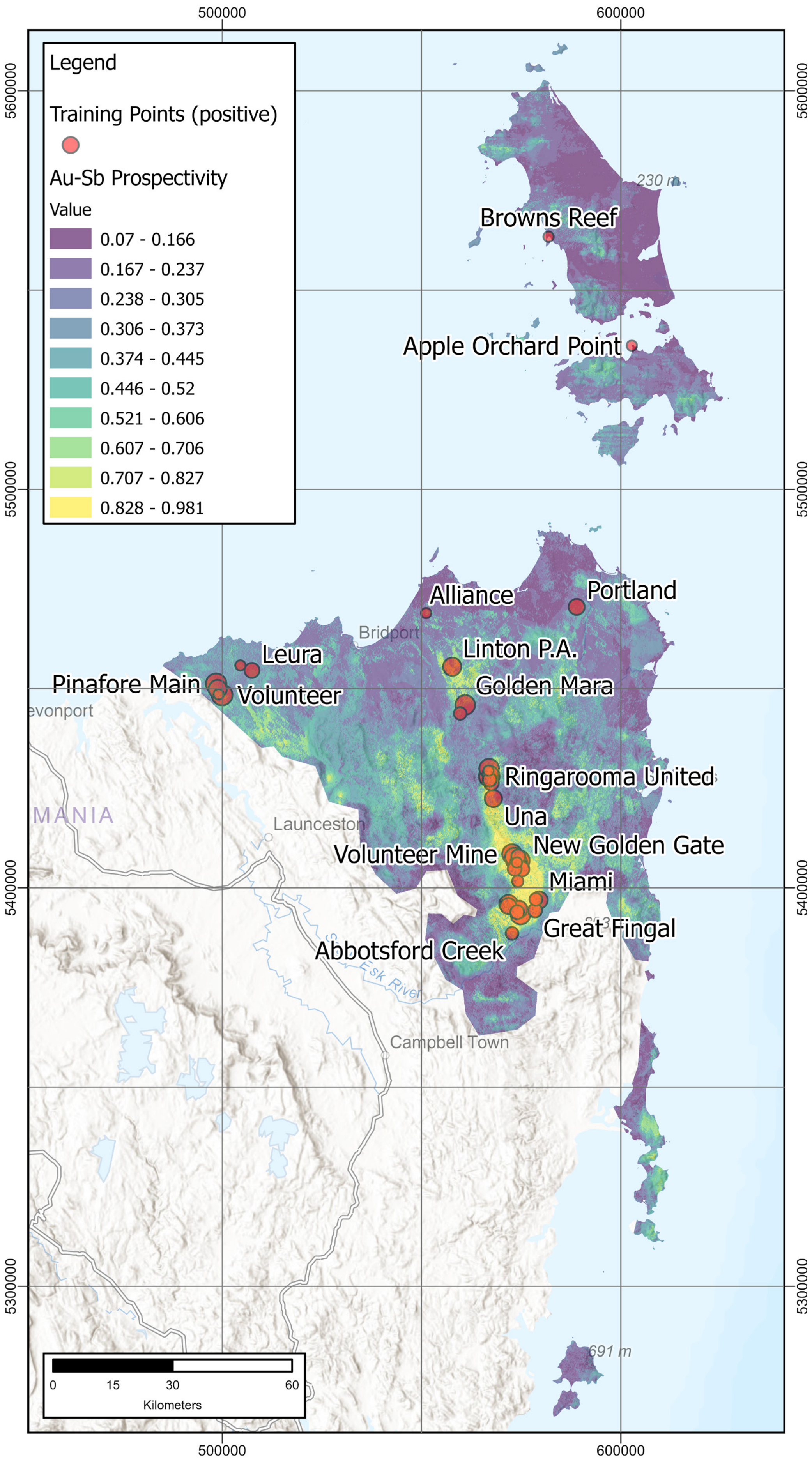

Figure 8. Model 1 mineral potential map showing relative prospectivity for turbidite-hosted gold-antimony mineralisation.

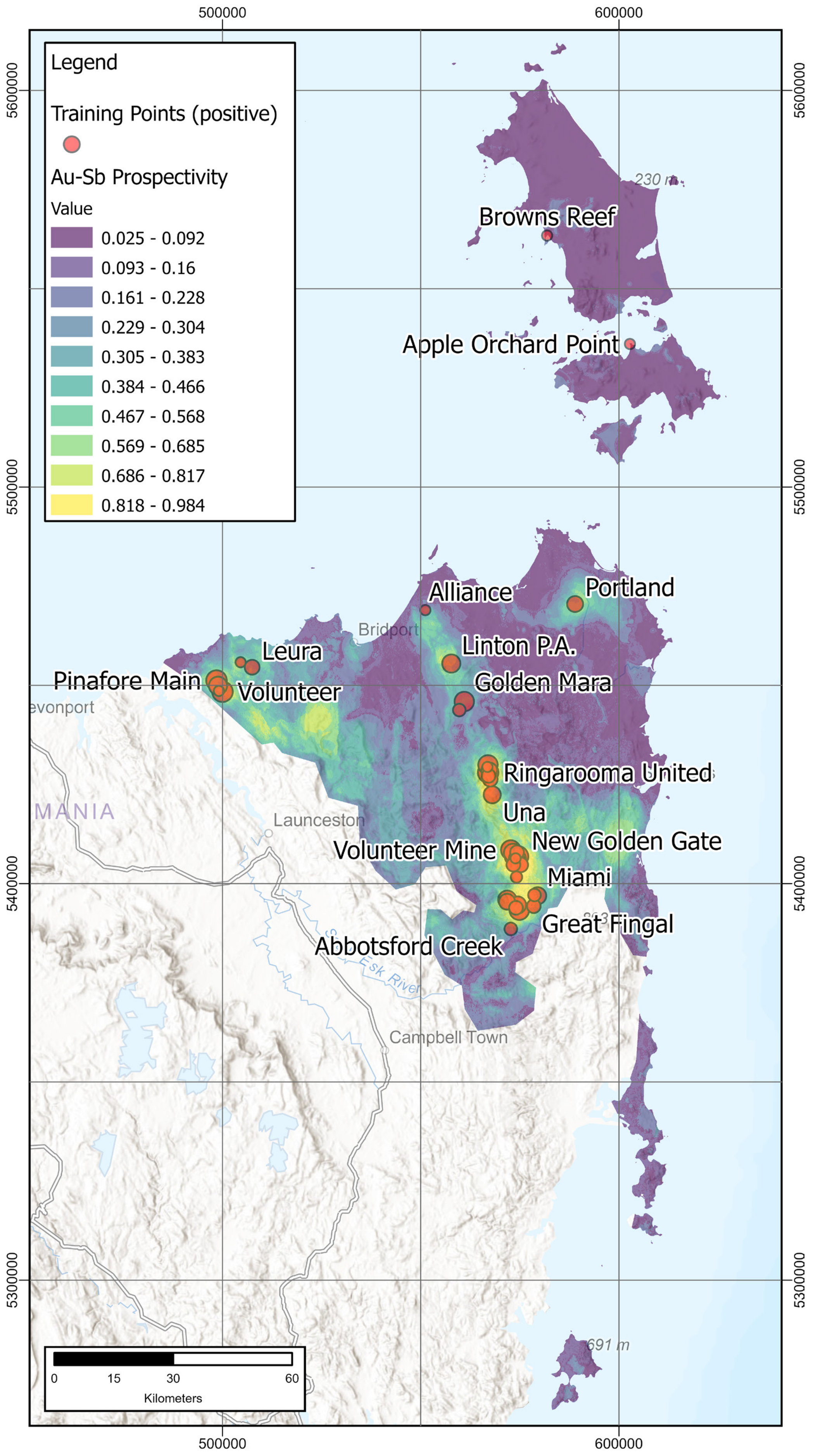

Figure 9. Model 2 mineral potential map showing relative prospectivity for turbidite-hosted gold-antimony mineralisation.

Both models highlight the Mangana-Mathinna-Alberton belt as the most prospective area in the region, which is consistent with present understanding of the mineral system and recorded endowments. This region corresponds to Mathinna Supergroup rocks with a high density of faulting, carbonaceous trap rocks, and anomalous stream geo-chemistry. Interestingly, Model 1 was able to highlight a similar area, relying mostly on textural magnetic maps and a gravity worm density map. Other regions highlighted by both models include Forester and Lefroy, both areas with significant historical gold production.

Model 2 assigns high prospectivity to the Lisle and Gladstone areas, which both contain historical gold mines, whereas these areas have low to moderate scores in Model 1. This indicates that these areas have distinct geophysical signatures than the Mangana-Mathinna-Alberton area where most of the positive training data are located.

The Furneaux Islands include moderately prospective areas in Model 1, some of which correspond to areas with known deposits. However, most of the islands are ascribed very low prospectivity scores in Model 2, likely due to a lack of 1:25 000 scale geological mapping, resulting in less mapped faults and observations of carbonaceous rocks and fault rocks. Similarly, the Freycinet Peninsula and Maria Island have some areas of moderate prospectivity in Model 1 that are relegated to unprospective in Model 2, due in part due to a lack of geochemical data.

One clear shortcoming of Model 1 is that some areas covered by granite are highlighted as prospective, which is inconsistent with mineral system knowledge. These areas either represent false positives due to the non-unique geophysical characteristics of the target mineral system, or they could represent targets where shallow granite covers prospective Mathinna Supergroup rocks.

Areas highlighted as prospective by Model 2 but lacking known deposits include an area of faulted Mathinna Supergroup rocks around Upper Scamander, as well as extensions to known gold fields.

Figures 10 and 11 show uncertainty maps for the two models. The standard deviation maps were derived from the ten forests comprising each ensemble and represent the variance associated with differences in negative training point sets. The Mahalanobis distance maps show the multivariate distance from each pixel to the mean of the training dataset, indicating how dissimilar a region is from the data seen by the model during training.

In Model 1, elevated standard deviation values occur primarily over granitic areas, indicating uncertainty in how the model classifies these rocks, likely due to overlapping geophysical characteristics with the Mathinna Supergroup rocks. Most of the predicted high prospectivity regions within the Mathinna Supergroup display low standard deviation values, providing greater confidence in these predictions. The moderately prospective regions of the Furneaux Islands are associated with higher standard deviations and should therefore be interpreted with more caution. Bright areas in the Mahalanobis distance map correspond to magnetic highs associated with Tertiary basalt and positive thorium anomalies related to several I-type granite plutons. Predictions over these areas should be treated with caution, as the model is extrapolating into parts of the feature space that were poorly represented in the training data.

Model 2 displays elevated standard deviation scores in halos surrounding some training points, suggesting that threshold buffer distances for geology maps, such as distance to carbonaceous rocks, vary depending on the choice of negative training points. Most highly prospective areas have low standard deviation values, indicating relatively stable predictions. However, the regions around Upper Scamander and the area between Mathinna and Alberton show both high prospectivity and high standard deviation, warranting careful interpretation. Between Mathinna and Alberton, Mathinna Supergroup rocks are covered by Permian sediments and Quaternary deposits, which may contribute to the increased prediction uncertainty, especially given the high contribution from radiometric maps. The Mahalanobis distance map again highlights distinctive magnetic and radiometric features, as well as several stream catchments containing anomalous arsenic concentrations. The Freycinet Peninsula and Maria Island also display elevated Mahalanobis distance values, due in part to the lack of carbonaceous rock and fault rock observations and the absence of stream geochemistry data. The lack of rock observations may reflect the absence of 1:25 000 scale geological mapping, rather than true absence of these features.

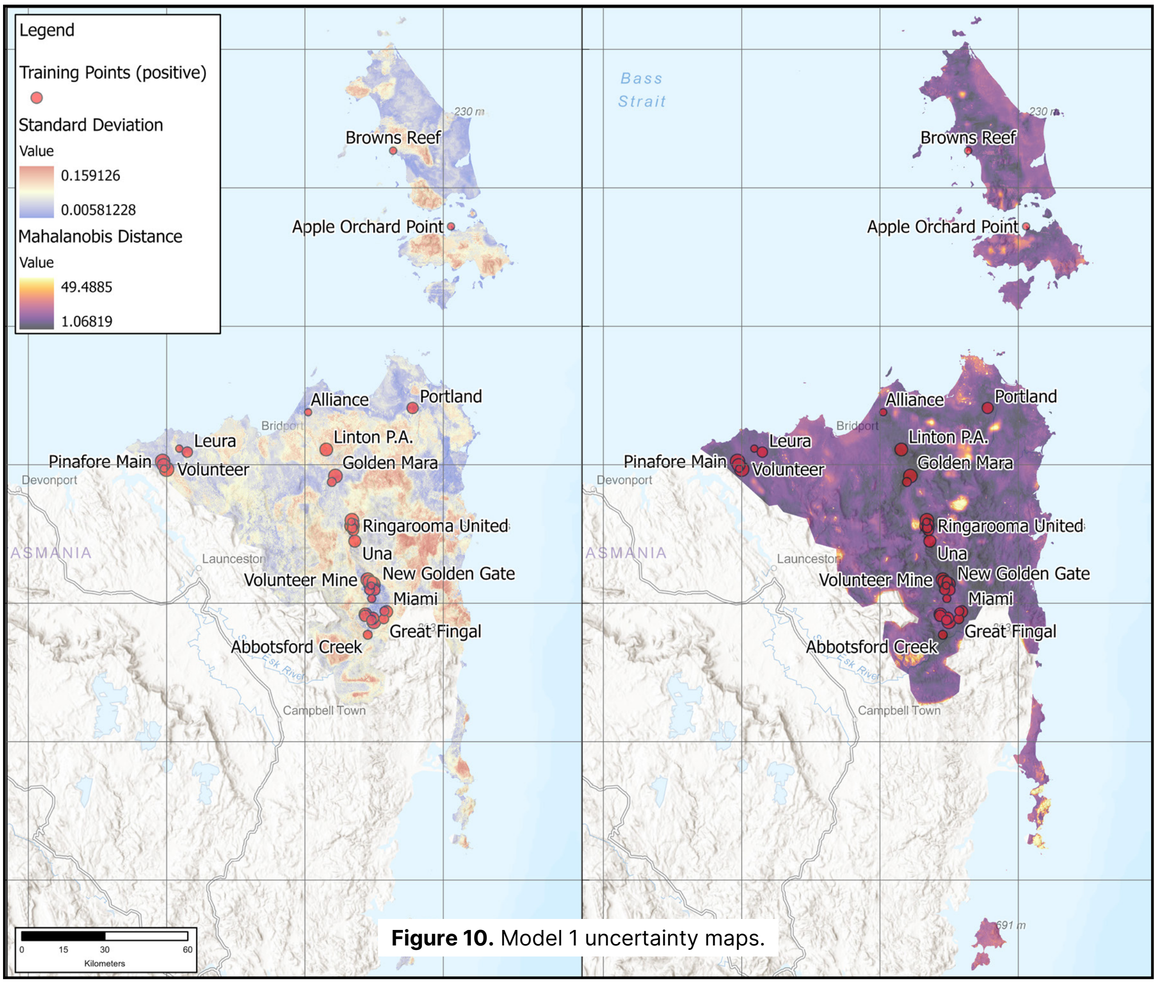

Figure 10. Model 1 uncertainty maps.

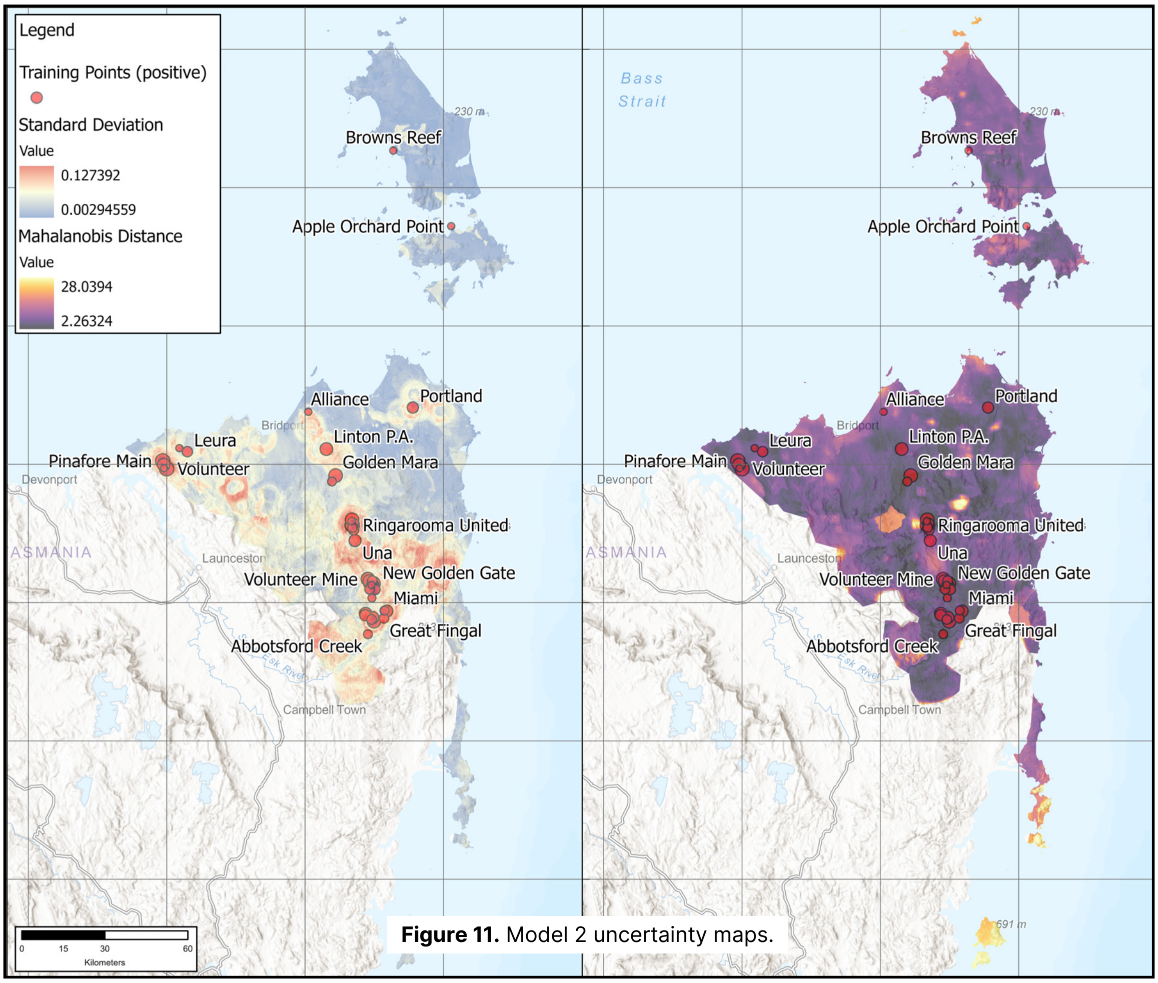

Figure 11. Model 2 uncertainty maps.

5.0 DISCUSSION

5.1 Model Performance and Geological Interpretation

The two models developed in this study effectively map the known mineral potential while also predicting new exploration targets. The ensemble random forest approach has provided an improvement in model performance and provides uncertainty metrics that improve the interpretability of the results.

The two-model approach provides complementary information. Model 1 (geophysics-only) highlights regional and greenfields targets based on objective and continuous datasets, while Model 2 incorporates all available data to refine targeting to highlight only the areas most likely to host mineralisation. While validation scores for Model 1 were lower than Model 2, Model 1 is more objective and has the potential to highlight prospectivity in under-explored regions.

The variables selected by the random forest algorithm are consistent with the turbidite-hosted Au-Sb mineral system model. High-importance predictors broadly relate to host rocks (e.g., Mathinna Supergroup, competency contrasts, carbonaceous rocks) and structures (e.g., mapped minor faults and fault rock observations). Variable importance scores can inform future exploration programs by identifying the most effective techniques for mapping this mineral system. For example, copper and arsenic stream sediment geochemistry were the most effective pathfinder elements at the scale of the modelling. Granite and granodiorite maps were tested initially but were excluded from the final models as the maps were essentially mirror images of the distance to Mathinna Supergroup map.

5.2 Novel Prospective Areas

Areas identified as prospective but lacking known deposits, such as Upper Scamander and a region around the Avenue River, warrant evaluation as potential exploration targets. However, these areas should be ground-truthed to distinguish genuine prospectivity from potential model artifacts. Several factors could explain these predictions: (1) genuine prospective geology with insufficient prior exploration, (2) geophysical signatures mimicking turbidite-hosted gold systems but representing different geological features, or (3) prediction bias toward data-rich areas. Field validation and integration with additional datasets would help resolve these ambiguities. For example, only limited rock chip and stream sediment sampling has been undertaken over the area and additional sampling could therefore rapidly provide a more accurate assessment of its true prospectivity.

5.3 Antimony Potential

Although antimony has not been historically produced from any of the gold mines in northeast Tasmania, comparisons with analogous deposits in Victoria suggest that there may be significant unrecognised potential. Minor stibnite has been reported from several gold-bearing quartz reefs at Lefroy, particularly at the Orlando mine and the Chum reef, where it occurs as massive and irregular bodies (Nye, 1941; Groves, 1965).

A review of the limited rock chip data across the study area shows that antimony anomalies of up to 430 ppm are concentrated within the Mathinna Supergroup. Several anomalies are located within a granite contact aureole adjacent to the Trafalgar gold deposit, which is interpreted as an intrusion-related gold system (Flynn Gold, 2024b). However, most anomalies fall within the turbidite-hosted Au-Sb prospectivity zones identified in this study. Antimony correlates most strongly with arsenic (r^2 = 0.67), gold (r^2 = 0.54), and lead (r^2 = 0.47), supporting an association with the turbidite-hosted gold system.

The scarcity of historical antimony analyses presents an opportunity to resample legacy drill core and determine whether economically significant antimony mineralisation is present in northeast Tasmania. The prospectivity maps developed in this study could be used as a framework to prioritise areas for resampling.

5.4 Limitations and Uncertainty

Limitations should be considered when interpreting the modelling results (below).

5.4.1 Data quality and coverage

Model 2 incorporates several geological datasets that contain inherent interpretative uncertainty, including rock type classifications and geological contact positions. A key limitation in the modelling is the absence of a statewide basement geology map, meaning that cover units unrelated to the target mineral system are included in the analysis. Buffering geological contacts and incorporating geophysical methods capable of detecting beneath cover partially mitigates this issue; however, artefacts associated with recent cover remain in the final model.

Structural datasets are affected by similar issues and are likely biased towards well-mapped regions. This was partially addressed by restricting inputs to regional-scale mapping data; however, coverage remains uneven. For example, Furneaux Islands have not yet been mapped at a 1:25 000 scale, resulting in relatively few mapped folds and faults compared with other areas of the study area. Detailed mapping is currently underway and the results from this work can be incorporated into future model updates. Folds were excluded from the current model despite being a recognised control on mineralisation due to highly selective mapping across the study area. Future work could include mapping fold hinges and faults from geophysical data to provide more consistent coverage of structural data over the study area. The recently completed statewide airborne electro-magnetic (AEM) survey, potentially in combination with recently acquired LIDAR data.

Geochemical datasets are also spatially biased, with denser sampling in areas of known mineralisation compared to greenfields or inaccessible areas. This may cause the models to underestimate prospectivity in underexplored areas.

5.4.2 Training Data

Positive training points may contain location errors or mineral system misclassifications, particularly for smaller or poorly understood mineral occurrences. To reduce the influence of these uncertainties, higher weights were assigned to larger, well-characterised deposits. A further challenge in the study area is the presence of intrusion-related gold deposits, which can be difficult to distinguish from the target turbidite-hosted mineral system. Expert knowledge was used to separate these deposit types, however uncertainty remains for some smaller occurrences where the classification is less certain. Recent work has demonstrated that these deposit types can be distinguished on the basis of apatite geochronology and geochemistry, providing a direction for future research (Siégel et al., 2026).

The generation of random negative training data also introduces uncertainty since some points may coincide with sites of unrecognised mineralisation. This issue was addressed through the ensemble random forest approach, which averages predictions across multiple training datasets and provides a measure of uncertainty associated with negative training point selection.

5.5 Exploration Implications

These models provide a first order targeting tool that can reduce exploration search space by over 85 %. The geophysics-only model is particularly valuable for greenfield exploration where geological and geochemical data are sparse, while the more complete Model 2 offers refined targeting in well-characterized terranes. Users should consider data coverage and quality when interpreting model outputs, particularly in data-sparse regions where predictions are less constrained.

5.6 Future Work

The methodology developed here allows models to be updated rapidly as new data become available or as machine learning methods evolve. For example, acquisition of airborne electro-magnetic data is currently underway across Tasmania, producing datasets that can be incorporated in model updates. Immediate applications include using the results to guide a core resampling program focussing on the antimony potential of the mineral system. Future work will focus on mapping the prospectivity of other critical mineral-bearing mineral systems across Tasmania, with ongoing refinement of the modelling workflow.

6.0 REFERENCES

Baillie, P. W. 1985. A Paleozoic suture in eastern Gondwanaland. *Tectonics*, 4:653–660.

Banks, M. R., Baillie, P. W. 1989. Late Cambrian to Devonian. *Geological Society of Australia Special Publication*, 15:182-237.

Barton, T. J. 1999. *Crustal Structure of Northeast Tasmania*, Australia. M.Sc. thesis, Monash University.

Berry, R. F., Everard, J. L., Bottrill, R. S., Meffre, S. 2025. Composition of pre-Carboniferous siliciclastic rocks in Tasmania. *Australian Journal of Earth Sciences,* 72:40-54.

Bierlein, F. P., Foster, D. A., Gray, D. R. 2005. Timing of orogenic gold mineralisation in northeastern Tasmania: implications for the tectonic and metallogenetic evolution of Palaeozoic SE Australia. *Mineralium Deposita*, 39:890–903.

Black, L. P., Everard, J. L., Mcclenaghan, M. P., Korsch, R. J., Calver, C. R. Fioretti, A. M., Brown, A. V., Foudoulis, C. 2010. Controls on Devonian–Carboniferous magmatism in Tasmania, based on inherited zircon age patterns, Sr, Nd and Pb isotopes, and major and trace element geochemistry. *Australian Journal of Earth Sciences*, 57:933-968.

Black, L. P., Mcclenaghan, M. P., Korsch, R. J., Everard, J. L., Foudoulis, C. 2005. The significance of Devonian–Carboniferous igneous activity in Tasmania, as derived from U–Pb SHRIMP dating of zircon. *Australian Journal of Earth Sciences*, 52:807–829.

Bottrill, R. S. 1991. Alluvial gold. *Geological Survey Mineral Resources*, 11.

Bottrill, R. S., Huston, D. L., Taheri, J., Zaw, K. 1992. Gold in Tasmania. *Bulletin Geological Survey Tasmania*, 70:24–46.

Breiman, L. 2001. Random forests. *Machine Learning*, 45:5–32.

Corbett, K. D., Quilty, P. G. M., Calver, C. R. 2014. *Geological Evolution of Tasmania*. Geological Society of Australia (Tasmania Division).

Carranza, E. J. M., Laborte, A. G. 2015. Random forest predictive modeling of mineral prospectivity with small number of prospects and data with missing values in Abra (Philippines). *Computational Geosciences*, 74:60–70.

Czertowicz, T. A. C. 2026. Prospectivity Mapping for Granite-related Tin-Tungsten-Fluorine-Rubidium Mineral Systems in Tasmania. *Technical Report*, Tasmanian Geological Survey 48.

Flynn Gold. 2024a. Exploration Target for Golden Ridge, NE Tasmania. Australian Stock Exchange.

Flynn Gold. 2024b. New High-Grade Gold Discovery at Golden Ridge, NE Tasmania. Grades up to 99.4g/t Au Recorded. Australian Stock Exchange.

Ford, A. 2020. Practical Implementation of Random Forest-Based Mineral Potential Mapping for Porphyry Cu–Au Mineralization in the Eastern Lachlan Orogen, NSW, Australia. *Natural Resources Research*, 29:267–283.

Goldfarb, R. J., Groves, D. I., Gardoll, S. 2001. Orogenic gold and geologic time: a global synthesis. *Ore Geology Reviews*, 18:1-2.

Groves, D. I. 1965. Geology of the Lefroy goldfield. *Geological Survey of Tasmania Explanatory Report*, TR9_58_76.

Groves, D. I. 1993. The crustal continuum model for late-Archean lode-gold deposits of the Yilgarn Block, Western Australia. *Mineralium Deposita*, 28:366-374.

Groves, D. I., Santosh, M., Wang, Q. 2024. The Boring Billion: A key to resolving controversy on ore-fluid source models for orogenic gold deposits? *Mineralium Deposita*, 59:435-444.

Holden, R. 2010. Annual Report 2008-2009 RL 2/2008. Cala Resources Pty Ltd [TCR 10_6042].

Kolb, J., Dziggel, A., Bagas, L. 2015. Hypozonal lode gold deposits: A genetic concept based on a review of the New Consort, Renco, Hutti, Hira Buddini, Navachab, Nevoria and The Granites deposits. *Precambrian Research*, 262:20-44.

Kreuzer, O. P., Roshanravan, R. 2025. Transforming LCT Pegmatite Targeting Models into AI-Powered Predictive Maps of Lithium Potential for Western Australia and Ontario: Approach, Results and Implications. *Minerals*, 15:397.

Leaman, D. E. 2012. An interpretation of the granitoid rocks of eastern Tasmania. *Mineral Resources Tasmania Geophysics Contractor Report,* 2012/01.

Leaman, D. E., Richardson, R. G. 2003. A geophysical model of the major Tasmanian granitoids. *Tasmanian Geological Survey Record*, 2003/11.

Nykanen, V., Lahti, I., Niiranen, T., Korhonen, K. 2015. Receiver operating characteristics (ROC) as validation tool for prospectivity models — A magmatic Ni–Cu case study from the Central Lapland Greenstone Belt, Northern Finland. *Ore Geology Reviews*, 71:853-860.

Nye, P. B. 1941. Antimony Minerals in Tasmania. *Geological Survey of Tasmania Explanatory Report*, 1941/24-25.

Patison, N. L., Berry, R. F., Davidson, G. J., Taylor, B. P., Bottrill, R. S., Manzi, B., Ryba, J., Shepherd, R. E. 2001. Regional metamorphism of the Mathinna Group, northeast Tasmania. *Australian Journal of Earth Sciences*, 48:281-292.

Phillips, G., Hughes, M. 1998. Victorian gold deposits. AGSO, *Journal of Australian Geology and Geophysics,* 17:213-216.

Reed, A. R. 2001. Pre-Tabberabberan deformation in eastern Tasmania: a southern extension of the Benambran Orogeny. *Australian Journal of Earth Sciences*, 48:785-796.

Reed, A. R. 2004. Gold mineralisation and the regional Palaeozoic structure of the Mathinna Supergroup, eastern Tasmania. *Tasmanian Geological Survey Record*, 2004/01.

Roach, M. J. 1992. Geology and geophysics of the Alberton-Mangana goldfield, northeast Tasmania. *Geological Survey Bulletin*, 70:199-207.

Roach, M. J. 1994. The regional geophysical setting of gold mineralisation in northeast Tasmania. Unpublished Ph.D. thesis, University of Tasmania. 179 pp.

Siégel, C., Pour, F. K., Cairns, C., Mcfarlane, H., Cayley, R., Pintér, Z., Verrall, M., Macrae, C., Walmsley, J., Boger, S., Lewis, J., Waugh, S. 2026. *Intrusion-related gold versus orogenic gold in northeast Victoria*. Final Project Report, MinEx CRC.

Seymour, D. B., Woolward, I. R., Mcclenaghan, M. P., Bottrill, R. S. 2011. Stratigraphic revision and re-mapping of the Mathinna Supergroup between the River Tamar and the Scottsdale Batholith, northeast Tasmania. Explanatory report for parts of the 1:25 000 scale Low Head, Tam O'Shanter, Weymouth, Retreat, Lilydale, Bridport, Bowood, Nabowla, Lisle and Patersonia map sheets. *Explanatory Report 1:25 000 Scale Digital Geological Map Series*, Mineral Resources Tasmania, 4

Taheri, J. 1993. Northeast Goldfields: A summary of the Alberton goldfield. *Tasmanian Geological Survey Record*, 1993/34.

Taheri, J., Bottrill, R. S. 1995. A study of the nature and origin of gold mineralisation, Mangana-Forester area, northeast Tasmania. *Geological Survey Bulletin*, 1994/05.

Taheri, J., Bottrill, R. S. 2005. Devonian granites and associated mineralisation in northeast and northwest Tasmania. *Geological Survey Bulletin*, 2005/03.

Wyborn, L. A. I., Heinrich, C. A., Jaques, A. L. 1994. Australian Proterozoic mineral systems: essential ingredients and mappable criteria. *Australian Institute of Mining and Metallurgy Publication Series,* 5:109-115.

Zhang, S., Carranza, E. J. M., Xiao, K., Wei, H., Yang, F., Chen, Z., Li, N., Xiang, J. 2022. Mineral prospectivity mapping based on isolation forest and random forest: Implication for the existence of spatial signature of mineralization in outliers. *Natural Resources Research*, 31.

APPENDIX 1

Data package resulting from this study

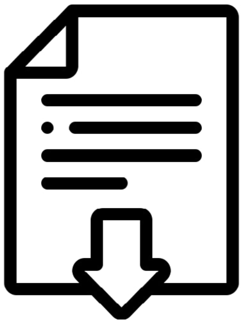

Download data

APPENDIX 2

Prospectivity Map

Download data

Tasmanian Government

Mineral Resources Tasmania
PO Box 56 Rosny Park
Tasmania Australia 7018

Phone: +61 3 6165 4800
Email: info@mrt.tas.gov.au
Web: www.mrt.tas.gov.au